Incorporating Heading Restrictions for Multilane-Road Target Tracking Using Radar Sensor

Yunlian Tian, Xi Cao, Wujun Li and Wei Yi
School of Information and Communication Engineering
University of Electronic Science and Technology of China, Chengdu, China
Email: {yunlian_tian; caoxi0419}@163.com; {1224liwujun; kussoyi}@gmail.com

***Abstract*—This paper intends to improve the multilane-road target tracking performance by considering heading restrictions. Most existing tracking algorithms assume that vehicles move independently in an open-field environment. However, the movements of vehicles have to be restricted by the geometry of roads, traffic rules, or preset routes. The effective utilization of prior knowledge regarding such restrictions can help to significantly enhance tracking performance. In this paper, we investigate the problem of state estimation while taking into account the heading restrictions imposed by the road direction. To describe the target longitudinal and lateral maneuvering behavior, we design the heading restrictions within a 2-D road coordinate system. The target state vector is then augmented by the y-intercept of the constraint straight line, and the measurement vector is augmented by constructing two pseudo-measurements. Consequently, the heading restrictions are incorporated into unscented Kalman filter based on two augmented vectors, called HR-UKF. Furthermore, we employ the singular value decomposition method to enhance numerical stability. Finally, the effectiveness of the proposed algorithm is validated through numerical simulations and real-measured data.**

***Index Terms*—Multilane-road target tracking, heading restrictions, 2-D road coordinate, pseudo-measurements, unscented Kalman filter.**

I. Introduction

Target tracking is one of the most important tasks in intelligent transportation systems [1], ground surveillance [2], and autonomous vehicles [3]. However, a common assumption in most current approaches is that the tracked traffic vehicle is permitted to move freely in an open-field environment. It poses a formidable challenge for traditional tracking algorithms to achieve robust on-road vehicle tracking. Proverbially, the motion of many targets is constrained by external physical limitations. For instance, land-based vehicles adhere to roadways [4], ships navigate predefined sea routes [5], and aircraft follow established flight paths. The external restrictions could be considered as prior information incorporated into the estimation process to enhance the tracking performance for the constrained targets [6], [7]. This paper aims to improve the vehicle tracking performance by leveraging prior knowledge of the road environment.

The problem of state estimation with equality constraints has been studied in recent years, and can be mainly classified into three categories. The first category converts the equality-constrained filtering problem into an unconstrained one. This approach offers the advantage of dimension reduction, often referred to as model reduction algorithms [6], [8], [9]. Nevertheless, the physical interpretation of the state components may not be convinced. The second category of algorithms is denominated as pseudo-measurement methodologies [10]–[12]. This methodology aims to augment the original measurements by seamlessly incorporating pseudo-measurements, employing equality constraints. Although implementing this structure is relatively straightforward with a clear interpretation, numerical issues may arise due to the singularity of the covariance matrix of the measurement noise [13]. The third category considers the original estimate result projected onto the constraint surface [7], [14]–[17]. However, as the projected point is in proximity to the unconstrained estimates rather than the true constrained state, these approaches do not yield the desired optimal estimate result.

Recently, the external physical restrictions have been introduced to formulate the equality constraints for state estimation. For instance, the destination restriction of the target is considered for state estimation [18]–[20], with the acknowledgment that only one point (i.e., the destination) on the restricted straight line can be precisely determined. The trajectory shape restriction on target motion is investigated in [10]. The problem of heading restrictions is first presented, and three pseudo-measurements are constructed to incorporate the heading constraint into the estimators in [12]. However, these restrictions [10], [12], [18]–[20] are only enforced on the longitudinal motion of the target, and the width of the roads is neglected. Furthermore, inspired by the social force model [21], [22], R. Ding *et al*. [23] extended it to vehicle tracking by integrating physical environmental restrictions into the tracking process. This extension involves considering the interactions between the dynamic model's noisy control input and the environment. Nevertheless, it still fails to account for lateral maneuvering behaviors such as lane changing.

To the best of our knowledge, the state estimation with equality constraints for vehicle tracking on multilane roads has received relatively little attention in the literature. As a result, building upon [12], this paper proposes a novel approach called HR-UKF to simultaneously consider the longitudinal and lateral maneuvering behaviors of vehicles on multilane roads. This solution incorporates heading restrictions into the unscented Kalman filter (UKF) within the 2-D road coordinate

This work was supported in part by the National Natural Science Foundation of China under Grant 62231008 and 62301127, in part by the China Postdoctoral Science Foundation under Grant BX20220057, 2023M730509 and GZB20230112, the "Tianfu Qingcheng" Plan of Sichuan Province under Grant1332 and 1395.

system [4]. The main contributions of this work are summarized as follows:

1) *Designs of heading restrictions:* The heading restrictions are designed using pseudo-measurements method in two typical situations, one is with a lane keeping, the other is a lane changing. For the lane keeping case, the pseudo-measurement is formulated by utilizing the equality relationship between position components of target state. For the case with lane changing, the pseudo-measurement is generated by considering the equality relationship between velocity components of target state. Next, the measurement vector is augmented by the two pseudo-measurements. Also, the target state vector is augmented by the y-intercept of the constraint straight line. Finally, the heading restrictions are incorporated into the tracking filter via the augmented state and measurement vectors.
2) *Tracking filter incorporating heading restrictions:* To tackle the strong nonlinearity between the augmented state and the augmented measurement, the unscented Kalman filter (UKF) [24] is employed. Moreover, the singular value decomposition method [25] is applied to improve the numerical stability resulting from singular measurement noise. The comprehensive performance assessments of the proposed HR-UKF method are conducted through numerical simulations and real-measured data, and the results confirm its effectiveness compared with the conventional UKF algorithm.

II. Target Models

A. Dynamic Model

In [4], the on-road motion of the target is represented in a 2-D road coordinate system, utilizing the traveled distance (mileage) coordinate s_k and its displacement from the central line d_k at index k. As illustrated in Fig. 1, the assumption is made that there are N lanes on the road, each with a width of 2Δ. The displacement d_k adheres to the constraint $|d_k| < N\Delta$. A point $P = (s_k, d_k)$ in the 2-D road coordinate system can be uniquely transformed into Cartesian coordinates (x_k, y_k) by

$$x_k = g_x(s_k, d_k) = x_0 + s_k \cos\alpha + d_k \sin\alpha, \tag{1}$$
$$y_k = g_y(s_k, d_k) = y_0 + s_k \sin\alpha - d_k \cos\alpha, \tag{2}$$

where s_k denotes the segment arc length between the starting point (x_0, y_0) and $P = (x_k, y_k)$, and d_k represents the signed distance between P and its orthogonal projection onto the centerline. The angle α is defined as the angle between the linear road segment and the X-axis.

According to (1), we can also derive as

$$s_k = g_s(x_k, y_k) = (x_k - x_0)\cos\alpha + (y_k - y_0)\sin\alpha, \tag{3}$$
$$d_k = g_d(x_k, y_k) = (x_k - x_0)\sin\alpha - (y_k - y_0)\cos\alpha. \tag{4}$$

In the 2-D road coordinate system, the vehicle's dynamic state can be separated into longitudinal and lateral motions,

$$\mathbf{x}_k = \begin{bmatrix}\mathbf{x}_l(k)\\ \mathbf{x}_d(k)\end{bmatrix} = \left[s_k, \dot{s}_k, \ddot{s}_k, d_k, \dot{d}_k, \ddot{d}_k\right]^\top, \tag{5}$$

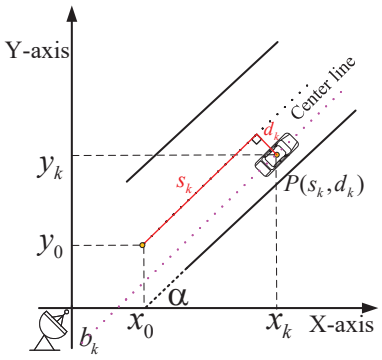

Fig. 1. The road-vehicle geometry. The black dot-dashed line represents the centerline of the road, while the pink dot-dashed line denotes the trajectory of the vehicle.

where $\dot{s}_k$ and $\ddot{s}_k$ denote the velocity and acceleration of longitudinal motion, and $\dot{d}_k$ and $\ddot{d}_k$ represent lateral speed and acceleration, respectively. The longitudinal and lateral states are straightforwardly given by

$$\mathbf{x}_l(k) = \left[s_k, \dot{s}_k, \ddot{s}_k\right]^\top, \quad \mathbf{x}_d(k) = \left[d_k, \dot{d}_k, \ddot{d}_k\right]^\top. \tag{6}$$

In the 2-D road coordinate system, the dynamic motion of a target is modeled as

$$\mathbf{x}_{k+1} = \mathbf{F}_k\mathbf{x}_k + \mathbf{\Gamma}_k\mathbf{v}_k, \tag{7}$$

where $\mathbf{F}_k$ denotes the state transition matrix, $\mathbf{\Gamma}_k$ is the process noise distribution matrix, $\mathbf{v}_k$ represents process noise accounting with covariance $\mathbf{q}_k$ for uncertainties in the prediction.

For the nearly constant acceleration (NCA) model, the state transition matrix and noise distribution matrix are given by

$$\mathbf{F}_k = \begin{bmatrix}1 & T & T^2/2\\ 0 & 1 & T\\ 0 & 0 & 1\end{bmatrix} \otimes \mathbf{I}_{2\times 2}, \mathbf{\Gamma}_k = \begin{bmatrix}T^2/2\\ T\\ 1\end{bmatrix} \otimes \mathbf{I}_{2\times 2}, \tag{8}$$

respectively, where T is the sampling interval and $\otimes$ denotes the Kronecker product, and $\mathbf{I}_{2\times 2}$ is a unit diagonal matrix with two dimensions.

Additionally, the process noise covariance matrix $\mathbf{q}_k = \mathrm{diag}\{\delta_s^2, \delta_d^2\}$, where δ_s and δ_d denote the standard deviations along the longitudinal and lateral directions, respectively.

B. Measurement Model

Assuming that the millimeter-wave radar provides measurements of the range r_k, the radial velocity v_k, and the azimuth θ_k. Thus, the model for the corresponding target-generated measurements is described as

$$\mathbf{z}_k = \begin{bmatrix}r_k\\ v_k\\ \theta_k\end{bmatrix} = h(\mathbf{x}_k) + \mathbf{w}_k \tag{9}$$

$$= \begin{bmatrix}\sqrt{g_x(s_k,d_k)^2 + g_y(s_k,d_k)^2}\\ \dfrac{g_x(s_k,d_k)\dot{g}_x(s_k,d_k) + g_y(s_k,d_k)\dot{g}_y(s_k,d_k)}{\sqrt{g_x(s_k,d_k)^2 + g_y(s_k,d_k)^2}}\\ \tan^{-1}\left(\dfrac{g_y(s_k,d_k)}{g_x(s_k,d_k)}\right)\end{bmatrix} + \mathbf{w}_k, \tag{10}$$

where $\dot{g}_x(s_k, d_k)$ and $\dot{g}_y(s_k, d_k)$ represent the derivatives with respect to the time variable. The function $h(\mathbf{x}_k)$ denotes the nonlinear vector-valued function, and $\mathbf{w}_k$ is zero-mean Gaussian noise in the measurement with variances δ_r^2, δ_v^2, and δ_θ^2, respectively. The covariance matrix of the measurement noise can be written as

$$\mathbf{R}_k = \begin{bmatrix} \delta_r^2 & 0 & 0 \\ 0 & \delta_v^2 & 0 \\ 0 & 0 & \delta_\theta^2 \end{bmatrix}. \tag{11}$$

For on-road vehicle targets, the movements of vehicles are influenced by the physical characteristics of the road. Specifically, the direction of vehicle movement is determined by the shapes of the road when navigating along a particular stretch. In this case, the anticipated direction of motion can be known in advance, and the target state is governed by an implicit restriction referred to as the heading restriction, imposed by the road. This paper aims to enhance tracking performance by integrating the heading restriction into tracking systems.

III. Designs of Heading Restrictions

In this section, we design the heading restrictions for two typical motion stages, namely, lane-keeping and lane-changing, on a straight-line multilane-road segment. For lane-keeping, the heading restriction is directly described by the equality relationship between the positions of the target state. In the case of lane-changing, both the positions and velocities of the target state are applied to formulate the heading restrictions. Next, to seamlessly integrate the heading restrictions into the tracking system, the state vector is augmented by the y-intercept, and two pseudo-measurements are generated to augment the measurement vector.

A. Pseudo-Measurement for Lane Keeping Stage

It is assumed that the target moves along a linear road segment, maintaining its current lane. The 2-D road-vehicle geometry with a heading of α is illustrated in Fig. 1. The pink dot-dashed line depicts the true trajectory of the vehicle, and the target's position in Cartesian coordinates at time step k is expressed as (x_k, y_k). During the lane keeping stage, the heading restriction can be designed as an equality constraint, relying on the restrictive relationship between the position components in Cartesian coordinates, namely,

$$y_k = \tan\alpha \cdot x_k + b_k, \tag{12}$$

where b_k represents the y-intercept at time step k.

While the restriction on the 2-D road coordinates system can be defined as

$$g_y(s_k, d_k) = \tan\alpha \cdot g_x(s_k, d_k) + b_k. \tag{13}$$

Remark 1: Note that the y-intercept b_k differs from the definition in the literature [12]. In our method, we purposely make the y-intercept b_k vary with each time step. This intentional choice is important because it prepares us to explain the heading restriction in detail during the next subsection, particularly in the context of lane-changing.

According to (13), the pseudo-measurement about the target state's position components can be designed as

$$\xi_k = g_y(s_k, d_k) - \tan\alpha \cdot g_x(s_k, d_k) - b_k. \tag{14}$$

B. Pseudo-Measurements for Lane Changing Stage

The act of lane changing involves the vehicle maneuvering across other lanes to enhance navigability by overtaking slower vehicles or evading obstructions.

Due to the non-compliance of the equality constraint (12) during lane changing, we assume that the lane-changing operation is executed through translational motion along the lateral direction in this paper. It can be equivalent to the constraint straight line having a movement speed $\dot{b}_k$ along the Y-axis. As depicted in Fig. 2, the heading of the vehicle remains constant during the lane-changing stage. The position restriction defined in (13) is still met. Therefore, we can further consider the velocity components to formulate the restriction relationship,

$$\dot{y}_k = \tan\alpha \cdot \dot{x}_k + \dot{b}_k, \tag{15}$$

where $\dot{y}_k$ and $\dot{x}_k$ represent velocities along the y-axis and x-axis in Cartesian coordinates, respectively. The term $\dot{b}_k$ denotes the velocity of the y-intercept.

In light of (13), the restriction relationship on the 2-D road coordinates system can be given by

$$\dot{g}_y(s_k, d_k) = \tan\alpha \cdot \dot{g}_x(s_k, d_k) + \dot{b}_k, \tag{16}$$

where $\dot{b}_k$ have

$$\dot{b}_k = \dot{d}_k \cdot \cos\alpha. \tag{17}$$

From (16) and (17), the pseudo-measurement about target state's velocity components is

$$\varrho_k = \dot{g}_y(s_k, d_k) - \tan\alpha \cdot \dot{g}_x(s_k, d_k) - \dot{b}_k. \tag{18}$$

C. Construction of Augmented Vectors

The road heading α is known in (14) and (18) as we have prior confirmation of the road geometry, while the y-intercept b_k varies with each time step. It can be deemed as an extra state component in target state vector.

Thus, the augmented state vector $\mathbf{x}_k^a$ can be written as

$$\mathbf{x}_k^a = \left[s_k, \dot{s}_k, \ddot{s}_k, d_k, \dot{d}_k, \ddot{d}_k, b_k\right]^\top. \tag{19}$$

In practical traffic scenarios, vehicles often undergo both lane-keeping and lane-changing maneuvers during traveling on the road. The two pseudo-measurements ξ_k and ϱ_k are

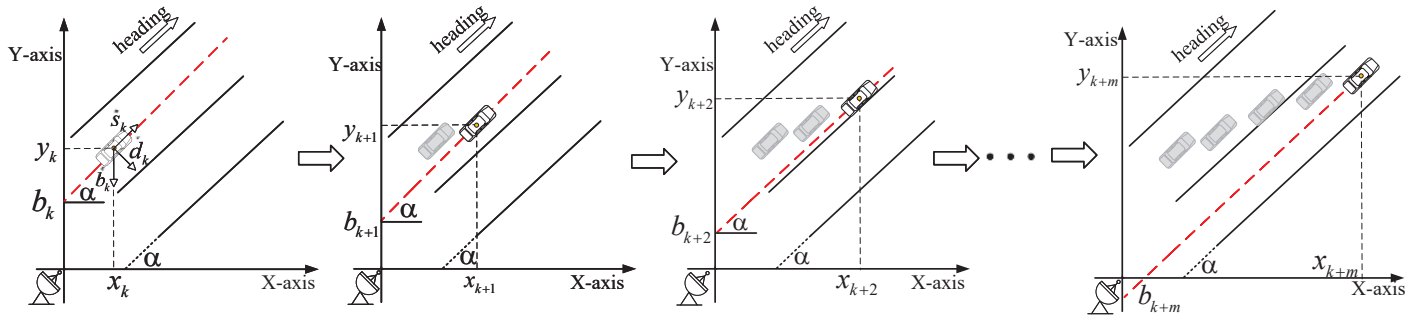

Fig. 2. Illustration of the lane-changing stage. The red dotted line illustrates the constrained straight line, which maintains a consistent incline angle but exhibits a changing y-intercept as time progresses. The shadow of the vehicle denotes its historical position during the lane change.

both incorporated into the augmented measurement model, as follows

$$\mathbf{z}_k^a = \begin{bmatrix} r_k \\ v_k \\ \theta_k \\ \xi_k \\ \varrho_k \end{bmatrix} = h^a(\mathbf{x}_k^a) + \mathbf{w}_k^a \tag{20}$$

$$= \begin{bmatrix} \sqrt{g_x(s_k,d_k)^2 + g_y(s_k,d_k)^2} \\ \dfrac{g_x(s_k,d_k)\dot{g}_x(s_k,d_k) + g_y(s_k,d_k)\dot{g}_y(s_k,d_k)}{\sqrt{g_x(s_k,d_k)^2 + g_y(s_k,d_k)^2}} \\ \tan^{-1}(\dfrac{g_y(s_k,d_k)}{g_x(s_k,d_k)}) \\ g_y(s_k,d_k) - \tan\alpha \cdot g_x(s_k,d_k) - b_k \\ \dot{g}_y(s_k,d_k) - \tan\alpha \cdot \dot{g}_x(s_k,d_k) - \dot{b}_k \end{bmatrix} + \mathbf{w}_k^a, \tag{21}$$

where $\mathbf{w}_k^a$ denotes augmented measurement noise with the augmented covariance matrix $\mathbf{R}_k^a$.

In principle, the pseudo-measurements ξ_k and ϱ_k are considered noise free as they are uncorrelated with the physical measurements r_k and θ_k. Consequently, the augmented covariance matrix $\mathbf{R}_k^a$ can be given by

$$\mathbf{R}_k^a = \mathbf{R}_k \oplus \mathbf{0}_{2\times 2}, \tag{22}$$

where $\oplus$ denotes the direct sum operation, and $\mathbf{0}_{2\times 2}$ represents the zero square matrix with two dimensions.

In light of (21), it is apparent that two types of equality constraints, imposed by the target direction, are incorporated into the measurement model, which play a crucial role in the tracking association and updating steps within the Kalman filter iteration.

IV. Tracking Filter Incorporating Heading Restrictions

In this section, we introduce a heading restrictions unscented Kalman filter (HR-UKF) method to improve tracking performance on a multilane road. The HR-UKF incorporates heading restrictions of the target within a 2-D road coordinate system. It's worth noting that other popular nonlinear filters, such as extended Kalman Filter (EKF) [26], [27] or cubature Kalman filter (CKF) [28], could also be considered as alternatives for addressing the nonlinear filtering problem.

As shown in (19), the base state vector $\mathbf{x}_k$ is augmented by the y-intercept b_k to formulate the restricted relationships (13) and (16). Consequently, based on (7) and (17), the augmented state equation model can be written as

$$\mathbf{x}_{k+1}^a = \mathbf{F}_k^a \mathbf{x}_k^a + \mathbf{\Gamma}_k^a \mathbf{v}_k$$
$$= \begin{bmatrix} \mathbf{F}_k & \mathbf{0}_{N_s\times 1} \\ \mathbf{0}_{1\times N_s-1} & T\cdot\cos\alpha \quad 1 \end{bmatrix} \cdot \begin{bmatrix} \mathbf{x}_k \\ b_k \end{bmatrix} + \begin{bmatrix} \mathbf{\Gamma}_k \\ \mathbf{0}_{1\times 2} \end{bmatrix} \mathbf{v}_k, \tag{23}$$

where N_s is the dimension of the base state vector $\mathbf{x}_k$.

Also, the augmented covariance of the process noise term in (23) can be written as

$$\mathbf{Q}^a = \mathbf{Q} \oplus \mathbf{0}_{1\times 1}, \tag{24}$$

where $\mathbf{Q} = \mathbf{\Gamma}_k \mathbf{q}_k \mathbf{\Gamma}_k^\top$ serves as base state transition process.

Building upon the augmented state equation (23) and the augmented measurement equation (21), the steps of the HR-UKF method are outlined as follows:

1) Initialization: Usually, the initial values for the target state and covariance are determined based on the first three measurements ($k = 1, 2, 3$) [29]. Thus, we transform the original radar measurements to construct the target state, employing unbiased measurement conversion method [30].

The initial values for the target state can be calculated as

$$\mathbf{x}_{k,k} = \begin{bmatrix} s_k \\ (s_k - s_{k-1})/T \\ (\dot{s}_k - \dot{s}_{k-1})/T \\ d_k \\ (d_k - d_{k-1})/T \\ (\dot{d}_k - \dot{d}_{k-1})/T \end{bmatrix}. \tag{25}$$

The unbiased conversion of original radar measurements to Cartesian coordinates can be expressed as

$$x_k = \mu_\theta r_k \cos\theta_k, y_k = \mu_\theta r_k \sin\theta_k, \tag{26}$$

where μ_θ denotes the bias compensation factor given by

$$\mu_\theta \equiv E(\cos w_k^\theta) = e^{-\delta_\theta^2/2}. \tag{27}$$

Substituting (26) and (27) into (3) and (4), we obtain

$$s_k = (\mu_\theta r_k \cos\theta_k - x_0)\cos\alpha + (\mu_\theta r_k \sin\theta_k - y_0)\sin\alpha, \tag{28}$$
$$d_k = (\mu_\theta r_k \cos\theta_k - x_0)\sin\alpha - (\mu_\theta r_k \sin\theta_k - y_0)\cos\alpha. \tag{29}$$

The initial covariance corresponding to target state $\mathbf{x}_{k,k}$ is given by

$$\mathbf{P}_{k,k}^{xx} = \begin{bmatrix} \mathbf{P}_{11,k} & \mathbf{P}_{12,k} \\ \mathbf{P}_{12,k}^{\top} & \mathbf{P}_{22,k} \end{bmatrix}, \tag{30}$$

where $\mathbf{P}_{k,k}^{xx}$ is a symmetric matrix, and the elements $\mathbf{P}_{11,k}$, $\mathbf{P}_{22,k}$, and $\mathbf{P}_{12,k}$ represent the converted measurement error matrix, and are derived based on [30].

From (25) and (19), the initial augmented state $\mathbf{x}_{k,k}^{a}$ can be given by

$$\mathbf{x}_{k,k}^{a} = \left[\mathbf{x}_{k,k}^{\top}, b_{k,k}\right]^{\top}. \tag{31}$$

In (31), the initial y-intercept $b_{k,k}$ is calculated as

$$b_{k,k} = y_0 - x_0 \tan\alpha - d_k\left(\cos\alpha + \sin\alpha\tan\alpha\right). \tag{32}$$

It is evident that the y-intercept $b_{k,k}$ is independent of s_k. Further, the initial augmented covariance corresponding to augmented state $\mathbf{x}_{k,k}^{a}$ is written as

$$\mathbf{P}_{k,k}^{x^a x^a} = \begin{bmatrix} \mathbf{P}_{k,k}^{xx} & \mathbf{P}_{k,k}^{xb} \\ (\mathbf{P}_{k,k}^{bx})^{\top} & P_{k,k}^{bb} \end{bmatrix}, \tag{33}$$

where $\mathbf{P}_{k,k}^{xb}$ is the initial cross-covariance between the base state $\mathbf{x}_k$ and y-intercept b_k, which is expressed as

$$\mathbf{P}_{k,k}^{xb} = \left[P_{k,k}^{sb}, P_{k,k}^{\dot{s}b}, P_{k,k}^{\ddot{s}b}, P_{k,k}^{db}, P_{k,k}^{\dot{d}b}, P_{k,k}^{\ddot{d}b}\right]^{\top}. \tag{34}$$

$$P_{k,k}^{bb} = \mathrm{var}[b_k \mid r_k, \theta_k]. \tag{35}$$

2) Generate Sigma Points: Due to the singularity of the measurement noise covariance (22), there may be an increased possibility of the state covariance being negatively defined. To improve the numerical stability of unscented transformation (UT) in UKF, the singular value decomposition of state covariance is used to generate the sigma points [25].

Definition 1: Let define

$$\sigma_i = \sqrt{\lambda_i((\mathbf{P}_{k,k}^{x^a x^a})^{\top}\mathbf{P}_{k,k}^{x^a x^a})}, i = 1, 2, \ldots, n \tag{36}$$

where σ_i denotes the singular value of $\mathbf{P}_{k,k}^{x^a x^a}$, $\lambda_i(\cdot)$ is the function to get the ith characteristic value of matrix.

Thus, the symmetrical positive semidefinite matrix $\mathbf{P}_{k,k}^{x^a x^a}$ can be decomposed as

$$\mathbf{P}_{k,k}^{x^a x^a} = \mathbf{U}\begin{bmatrix} \mathbf{D} & 0 \\ 0 & 0 \end{bmatrix}\mathbf{V}, \tag{37}$$

where $\mathbf{U}$ and $\mathbf{V}$ are unitary matrix, and $\mathbf{D}$ is a diagnal matrix with all the nonzero singular values of $\mathbf{P}_{k,k}^{x^a x^a}$, i.e.,

$$\mathbf{D} = \mathrm{diag}(\sigma_1, \sigma_2, \ldots, \sigma_n). \tag{38}$$

Instantiating (38) into UT processing, the sigma points can be calculated as

$$\mathcal{X}_{k,k}^{0} = \mathbf{x}_{k,k}^{a} \tag{39}$$

$$\mathcal{X}_{k,k}^{j} = \mathbf{x}_{k,k}^{a} + \left[\mathbf{U}\sqrt{(N_s^x+\lambda)\mathbf{D}}\mathbf{U}^{\top}\right]_j, j = 1, \ldots, N_s^x \tag{40}$$

$$\mathcal{X}_{k,k}^{j} = \mathbf{x}_{k,k}^{a} - \left[\mathbf{U}\sqrt{(N_s^x+\lambda)\mathbf{D}}\mathbf{U}^{\top}\right]_{j-N_s^x}, \quad j = N_s^x+1, \ldots, 2N_s^x \tag{41}$$

where N_s^x represents the dimension of the augmented state vector $\mathbf{x}_k^a$.

3) Calculate the Predicted State $\mathbf{x}_{k+1,k}^{a}$ and Associated Covariance $\mathbf{P}_{k+1,k}^{x^a x^a}$:

$$(\mathcal{X}_{k,k}^{j})^{*} = \mathbf{F}_k^a \mathcal{X}_{k,k}^{j}, \qquad \mathbf{x}_{k+1,k}^{a} = \sum_{j=0}^{2N_s^x} w_j^{(m)} (\mathcal{X}_{k,k}^{j})^{*}, \tag{42}$$

$$\mathbf{P}_{k+1,k}^{x^a x^a} = \sum_{j=0}^{2N_s^x} w_j^{(c)} ((\mathcal{X}_{k,k}^{j})^{*} - \mathbf{x}_{k+1,k}^{a})((\mathcal{X}_{k,k}^{j})^{*} - \mathbf{x}_{k+1,k}^{a})^{\top} + \mathbf{Q}^a, \tag{43}$$

where $w_j^{(m)}$ and $w_j^{(c)}$ is given by

$$w_0^{(m)} = \frac{\lambda}{N_s^x + \lambda}, w_0^{(c)} = \frac{\lambda}{N_s^x + \lambda} + (1 - \zeta^2 + \beta), \tag{44}$$

$$w_j^{(m)} = w_j^{(c)} = \frac{1}{2(N_s^x + \lambda)}, j = 1, ..., 2N_s^x, \tag{45}$$

where $\lambda = (N_s^x + \kappa)\zeta^2 - N_s^x$, where ζ represents the control factor for sigma point distribution, κ is a scaling parameter, and β is a nonnegative constant.

4) Update:

$$\mathcal{Y}_{k,k}^{j} = h^a((\mathcal{X}_{k,k}^{j})^{*}), \qquad \mathbf{y}_{k+1,k}^{a} = \sum_{j=0}^{2N_s^x} w_j^{(m)} \mathcal{Y}_{k,k}^{j}, \tag{46}$$

$$\mathbf{S}^a = \sum_{j=0}^{2N_s^x} w_j^{(c)} (\mathcal{Y}_{k,k}^{j} - \mathbf{y}_{k+1,k}^{a})(\mathcal{Y}_{k,k}^{j} - \mathbf{y}_{k+1,k}^{a})^{\top} + \mathbf{R}^a, \tag{47}$$

$$\mathbf{G}^a = \sum_{j=0}^{2N_s^x} w_j^{(c)} ((\mathcal{X}_{k,k}^{j})^{*} - \mathbf{x}_{k+1,k}^{a})(\mathcal{Y}_{k,k}^{j} - \mathbf{y}_{k+1,k}^{a})^{\top}, \tag{48}$$

$$\mathbf{K}_{k+1}^{a} = \mathbf{G}^a(\mathbf{S}^a)^{-1}, \tag{49}$$

$$\mathbf{P}_{k+1,k+1}^{x^a x^a} = \mathbf{P}_{k+1,k}^{x^a x^a} - \mathbf{K}_{k+1}^{a}\mathbf{S}^a(\mathbf{K}_{k+1}^{a})^{\top}, \tag{50}$$

$$\mathbf{x}_{k+1,k+1}^{a} = \mathbf{x}_{k+1,k}^{a} + \mathbf{K}_{k+1}^{a}(\mathbf{z}_k^a - h^a(\mathbf{x}_{k+1,k}^{a})). \tag{51}$$

V. Simulations and Real-measured Data Process

In this section, both numerical simulations and real-measured data are provided to validate the effectiveness of the proposed HR-UKF method. Due to Zhang *et al.* [12] not considering the problem of multiland-road vehicle tracking, the proposed method is only compared to the traditional UKF tracking algorithm.

A. Numerical Simulations

The performance of the proposed HR-UKF algorithm is analyzed for two different scenarios with the target traveling at nearly constant velocity. The parameter settings for the scenarios are as follows: sampling time $T = 1$ s; process noise standard deviation of the tracker $\delta_s = 0.5$ m/s, $\delta_d = 0.5$ m/s; slant angle of the lane $\alpha = 1.5342\,\mathrm{deg}$; measurement noise $\delta_r = 2$ m, $\delta_v = 1$ m/s, $\delta_\theta = 0.15$ degrees; spatial density of false alarms $\lambda_\phi = 5 \times 10^{-3}$; detection probability $P_d = 0.95$. The UKF-related parameters are $\zeta = 1$, $\kappa = 2$, $\beta = 2$.

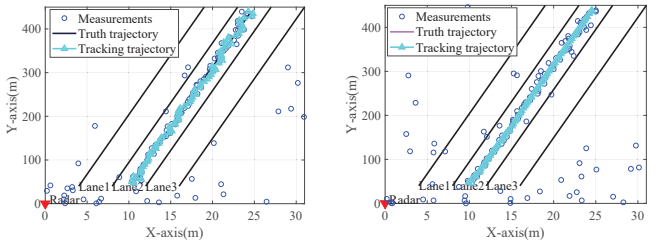

(a) (b)

Fig. 3. Illustration of the tracking results for different method in Scenario 1. (a) The traditional UKF method. (b) The proposed HR-UKF method.

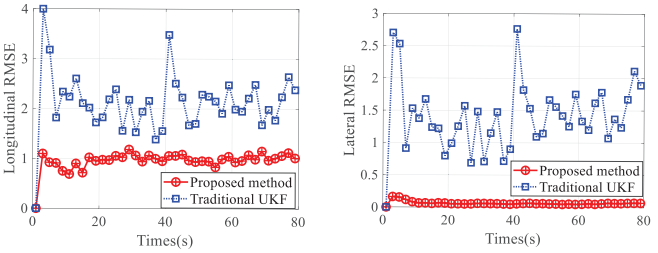

(a) (b)

Fig. 4. The RMSE performance of longitudinal and lateral motion in Scenario 1. (a) The RMSE of longitudinal motion. (b) The RMSE of lateral motion.

The first (Scenario 1) and second (Scenario 2) scenarios consist of $N = 3$ lanes, each having a width of $2\Delta = 4m$. In Scenario 1, the target travels on the road (from bottom to top) while maintaining a constant velocity and staying in the current lane. In Scenario 2, the target undergoes lane changes (from left to right) two times during the simulated duration.

1) Scenario 1

In the Cartesian coordinate system, the parameter settings are as follows: the initial sensor location is $[0\ \text{m}, 0\ \text{m}]$; the starting point of the road segment is $x_0 = y_0 = 0$ m; the target's initial location is $[10\ \text{m}, 40\ \text{m}]$; the target's initial velocity is $[10\ \text{m/s}, \frac{5}{\tan\alpha}\ \text{m/s}]$; the target's initial acceleration is $[0\ \text{m/s}^2, 0\ \text{m/s}^2]$.

Fig. 3 illustrates the truth trajectory and the tracking results of different methods for a sample run. It can be intuitively seen that the proposed HR-UKF method demonstrates enhanced tracking stability, with reduced track jitter. This is a result of incorporating heading restrictions into the UKF tracking framework, enhancing both track association and updates.

Fig. 4 illustrates the RMSE performance of longitudinal and lateral motion after 100 Monte Carlo runs. A comparison of the position RMSE between two methods reveals that the traditional UKF tracking algorithm exhibits poor position estimates, attributed to its failure to consider heading restrictions. In contrast, the proposed HR-UKF tracking algorithm demonstrates improved tracking accuracy.

2) Scenario 2

In this scenario, the target undergoes two lane changes at time steps $k = 25$ s and $k = 55$ s. Fig. 5 and Fig. 6 display the tracking results and the position RMSE performance in longitudinal and lateral motion. It is evident that the proposed HR-UKF method outperforms the traditional UKF method in terms of the tracked trajectory and position RMSE.

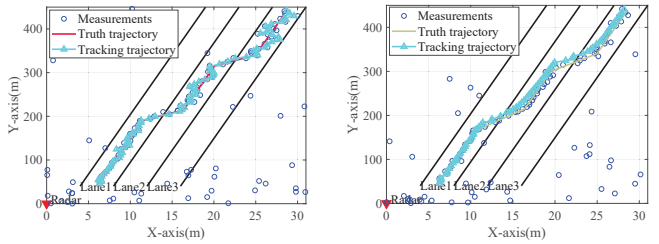

(a) (b)

Fig. 5. Illustration of the tracking results for different method in Scenario 1. (a) The traditional UKF method. (b) The proposed HR-UKF method.

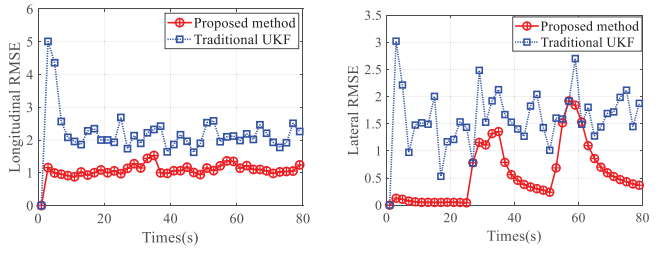

(a) (b)

Fig. 6. The RMSE performance of longitudinal and lateral motion in Scenario 1. (a) The RMSE of longitudinal motion. (b) The RMSE of lateral motion.

Additionally, as depicted in Fig. 6(b), the tracking error in lateral motion may increase during lane changes. This outcome is reasonably explained by the impact of hysteretic track updates. Specifically, the state covariance of target track converges to a relatively small value before the lane changing stage. However, the track state fails to update promptly at the onset of a lane change, leading to an increase in tracking error.

B. Real-measured Data Process

To further validate the excellent tracking performance of the proposed HR-UKF method, the real-measured data process is conducted.

The depicted realistic traffic scene in Fig. 7(a) and Fig. 8(a) unfolds at a traffic light intersection. Within this dynamic environment, various vehicles navigate either along their current lane or make lane changes. [1]

As depicted in Fig. 7, a comparison of trajectories in the far region of the radar reveals that the proposed HR-UKF tracking algorithm outperforms the traditional UKF method in terms of both tracking accuracy and smoothness. Due to measurement jitter in the far region of the radar's field of view, the quality of tracks produced by the traditional UKF method has been severely degraded. Moreover, multi-vehicle tracking is investigated as shown in Fig. 8. In this scene, one vehicle keeps moving in its current lane, while another vehicle initiates a lane change at approximately 120 m (crossing from lane 1 to lane 2). Notably, the UKF tracking algorithm exhibits tracking errors, and even incurs cross-lane inaccuracies.

In conclusion, the proposed HR-UKF algorithm effectively enhances the quality of multilane-road vehicle tracking.

[1]This study specifically focuses on precisely tracking actively moving vehicles, deliberately excluding tracks associated with vehicles displaying a move-stop pattern from our consideration.

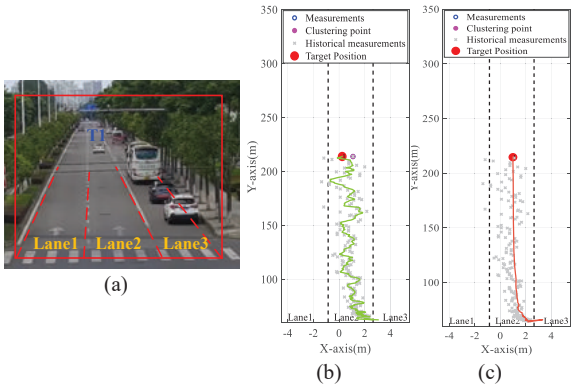

Fig. 7. Illustration of tracking result of real-measured data processing. (a) Realistic traffic scene. (b) Traditional UKF. (c) The proposed HR-UKF.

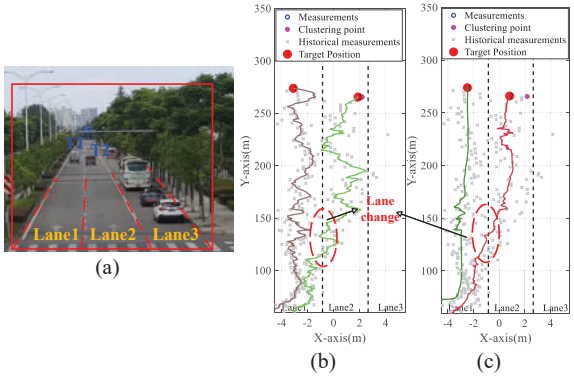

Fig. 8. Illustration of tracking result of real-measured data processing. (a) Realistic traffic scene. (b) Traditional UKF. (c) The proposed HR-UKF.

VI. Conclusions

This paper proposes an HR-UKF tracking algorithm for multilane-road target tracking in a 2D road coordinate system, incorporating heading restrictions into the Kalman filter framework. Two typical situations, lane keeping and lane changing, are investigated in this work, wherein two pseudo-measurements are constructed, resorting to the constrained relationship between position and velocity elements. In both situations, the tracking performance is significantly improved in terms of longitudinal and lateral motion compared with the traditional UKF algorithm.

References

[1] H. Zhu, K.-V. Yuen, L. Mihaylova, and H. Leung, "Overview of environment perception for intelligent vehicles," *IEEE Trans. Intell. Transp. Syst.*, vol. 18, no. 10, pp. 2584–2601, 2017.

[2] M. Ulmke and W. Koch, "Road-map assisted ground moving target tracking," *IEEE Trans. Aerosp. Electron. Syst.*, vol. 42, no. 4, pp. 1264–1274, 2006.

[3] X. Cao, C. Zhu, and W. Yi, "PHD filter based traffic target tracking framework with FMCW radar," in *Proc. 11th Int. Conf. Control, Autom. Inf. Sci. (ICCAIS)*. IEEE, 2022, pp. 468–475.

[4] Y. Chen, V. P. Jilkov, and X. R. Li, "Multilane-road target tracking using radar and image sensors," *IEEE Trans. Aerosp. Electron. Syst.*, vol. 51, no. 1, pp. 65–80, 2015.

[5] L. Xu, Y. Liang, Z. Duan, and G. Zhou, "Route-based dynamics modeling and tracking with application to air traffic surveillance," *IEEE Trans. Intell. Transp. Syst.*, vol. 21, no. 1, pp. 209–221, 2019.

[6] R. J. Hewett, M. T. Heath, M. D. Butala, and F. Kamalabadi, "A robust null space method for linear equality constrained state estimation," *IEEE Trans. Signal Process.*, vol. 58, no. 8, pp. 3961–3971, 2010.

[7] D. Simon and T. L. Chia, "Kalman filtering with state equality constraints," *IEEE Trans. Aerosp. Electron. Syst.*, vol. 38, no. 1, pp. 128–136, 2002.

[8] A. Pizzinga, "Constrained kalman filtering: additional results," *Int. Stat. Rev.*, vol. 78, no. 2, pp. 189–208, 2010.

[9] D. Simon, "Kalman filtering with state constraints: a survey of linear and nonlinear algorithms," *IET Control. Theory. Appl.*, vol. 4, no. 8, pp. 1303–1318, 2010.

[10] G. Zhou, K. Li, X. Chen, L. Wu, and T. Kirubarajan, "State estimation with a destination constraint using pseudo-measurements," *Signal Process.*, vol. 145, pp. 155–166, 2018.

[11] Z. Tian, M. Cen, Y. Li, and H. Zhu, "Ground vehicle tracking using context-based sojourn time dependent markov model and pseudo-measurement," *IEEE Access*, vol. 8, pp. 111 536–111 552, 2020.

[12] Z. Zhang, K. Li, and G. Zhou, "State estimation with heading constraints for on-road vehicle tracking," *IEEE Trans. Intell. Transp. Syst.*, vol. 23, no. 8, pp. 13 614–13 635, 2021.

[13] Z. Duan and X. R. Li, "The role of pseudo measurements in equality-constrained state estimation," *IEEE Trans. Aerosp. Electron. Syst.*, vol. 49, no. 3, pp. 1654–1666, 2013.

[14] C. Yang and E. Blasch, "Kalman filtering with nonlinear state constraints," *IEEE Trans. Aerosp. Electron. Syst.*, vol. 45, no. 1, pp. 70–84, 2009.

[15] S. J. Julier and J. J. LaViola, "On kalman filtering with nonlinear equality constraints," *IEEE Trans. Signal Process.*, vol. 55, no. 6, pp. 2774–2784, 2007.

[16] K. Li, G. Zhou, and L. Xu, "Fixed-lag smoothing with linear equality constraints," in *Proc. 20th Int. Conf. Inf. Fusion (Fusion)*. IEEE, 2017, pp. 1–8.

[17] R. Jiang, H. Zhou, H. Wang, and S. S. Ge, "Road-constrained geometric pose estimation for ground vehicles," *IEEE Trans. Autom. Sci.*, vol. 17, no. 2, pp. 748–760, 2019.

[18] G. Zhou and K. Li, "State estimation with destination constraints," in *Proc. 19th Int. Conf. Inf. Fusion (Fusion)*. IEEE, 2016, pp. 292–297.

[19] Y. Huang, X. Wang, Y. Guo, and W. An, "State estimation with incomplete linear constraint," in *Proc. 20th Int. Conf. Inf. Fusion (Fusion)*. IEEE, 2017, pp. 1–6.

[20] G. Zhou, K. Li, and T. Kirubarajan, "Constrained state estimation using noisy destination information," *Signal Process.*, vol. 166, p. 107226, 2020.

[21] A. Ur-Rehman, S. M. Naqvi, L. Mihaylova, and J. A. Chambers, "Multi-target tracking and occlusion handling with learned variational bayesian clusters and a social force model," *IEEE Trans. Signal Process.*, vol. 64, no. 5, pp. 1320–1335, 2015.

[22] P. Feng, W. Wang, S. Dlay, S. M. Naqvi, and J. Chambers, "Social force model-based mcmc-ocsvm particle PHD filter for multiple human tracking," *IEEE Trans. Multimedia*, vol. 19, no. 4, pp. 725–739, 2016.

[23] R. Ding, M. Yu, H. Oh, and W.-H. Chen, "New multiple-target tracking strategy using domain knowledge and optimization," *IEEE Trans. Syst. Man Cybern.: Syst.*, vol. 47, no. 4, pp. 605–616, 2016.

[24] S. Julier, J. Uhlmann, and H. F. Durrant-Whyte, "A new method for the nonlinear transformation of means and covariances in filters and estimators," *IEEE Trans. Autom. Control*, vol. 45, no. 3, pp. 477–482, 2000.

[25] Y. Ma, Z. Wang, X. Zhao, J. Han, and Y. He, "A UKF algorithm based on the singular value decomposition of state covariance," in *Proc. 8th World Congr. Intelligent Control Autom. (WCICA)*. IEEE, 2010, pp. 5830–5835.

[26] T. Song and J. Speyer, "A stochastic analysis of a modified gain extended kalman filter with applications to estimation with bearings only measurements," *IEEE Trans. Autom. Control*, vol. 30, no. 10, pp. 940–949, 1985.

[27] N. Cui, L. Hong, and J. R. Layne, "A comparison of nonlinear filtering approaches with an application to ground target tracking," *Signal Process.*, vol. 85, no. 8, pp. 1469–1492, 2005.

[28] I. Arasaratnam and S. Haykin, "Cubature kalman filters," *IEEE Trans. Autom. Control*, vol. 54, no. 6, pp. 1254–1269, 2009.

[29] Y. Bar-Shalom, X. R. Li, and T. Kirubarajan, *Estimation With Applications to Tracking and Navigation: Theory Algorithms and Software*. John Wiley & Sons, 2004.

[30] S. Bordonaro, P. Willett, and Y. Bar-Shalom, "Decorrelated unbiased converted measurement kalman filter," *IEEE Trans. Aerosp. Electron. Syst.*, vol. 50, no. 2, pp. 1431–1444, 2014.